Biomedical Optics EXPRESS

# Portable handheld diffuse reflectance spectroscopy system for clinical evaluation of skin: a pilot study in psoriasis patients

**Shih-Yu Tzeng,[1] Jean-Yan Guo,[1] Chao-Chun Yang,[2] Chao-Kai Hsu,[2] Hung Ji Huang,[3] Shih-Jie Chou,[3] Chi-Hung Hwang,[3] and Sheng-Hao Tseng[1,4,*]**

[1]*Department of Photonics, National Cheng Kung University, Tainan, 701, Taiwan*
[2]*Department of Dermatology, National Cheng Kung University Hospital, College of Medicine, National Cheng Kung University, Tainan, 701, Taiwan*
[3]*Instrument Technology Research Center, National Applied Research Laboratories, Hsinchu, 300, Taiwan*
[4]*Advanced Optoelectronic Technology Center, National Cheng Kung University, Tainan, 701, Taiwan*
[*]*stseng@mail.ncku.edu.tw*

**Abstract:** Diffuse reflectance spectroscopy (DRS) has been utilized to study biological tissues for a variety of applications. However, many DRS systems are not designed for handheld use and/or relatively expensive which limit the extensive clinical use of this technique. In this paper, we report a handheld, low-cost DRS system consisting of a light source, optical switch, and a spectrometer, that can precisely quantify the optical properties of tissue samples in the clinical setting. The handheld DRS system was employed to determine the skin chromophore concentrations, absorption and scattering properties of 11 patients with psoriasis. The measurement results were compared to the clinical severity of psoriasis as evaluated by dermatologist using PASI (Psoriasis Area and Severity Index) scores. Our statistical analyses indicated that the handheld DRS system could be a useful non-invasive tool for objective evaluation of the severity of psoriasis. It is expected that the handheld system can be used for the objective evaluation and monitoring of various skin diseases such as keloid and psoriasis.



**OCIS codes:** (170.1610) Clinical applications; (170.3660) Light propagation in tissues.

## References and links

1. D. J. Cappon, T. J. Farrell, Q. Fang, and J. E. Hayward, "Fiber-optic probe design and optical property recovery algorithm for optical biopsy of brain tissue," J. Biomed. Opt. **18**(10), 107004 (2013).
2. A. Cerussi, N. Shah, D. Hsiang, A. Durkin, J. Butler, and B. J. Tromberg, "In vivo absorption, scattering, and physiologic properties of 58 malignant breast tumors determined by broadband diffuse optical spectroscopy," J. Biomed. Opt. **11**(4), 044005 (2006).
3. C. K. Hsu, S. Y. Tzeng, C. C. Yang, J. Y. Lee, L. L. Huang, W. R. Chen, M. Hughes, Y. W. Chen, Y. K. Liao, and S. H. Tseng, "Non-invasive evaluation of therapeutic response in keloid scar using diffuse reflectance spectroscopy," Biomed. Opt. Express **6**(2), 390–404 (2015).
4. A. Kim, M. Roy, F. Dadani, and B. C. Wilson, "A fiberoptic reflectance probe with multiple source-collector separations to increase the dynamic range of derived tissue optical absorption and scattering coefficients," Opt. Express **18**(6), 5580–5594 (2010).
5. R. Nachabé, D. J. Evers, B. H. Hendriks, G. W. Lucassen, M. van der Voort, J. Wesseling, and T. J. Ruers, "Effect of bile absorption coefficients on the estimation of liver tissue optical properties and related implications in discriminating healthy and tumorous samples," Biomed. Opt. Express **2**(3), 600–614 (2011).
6. Q. Liu and N. Ramanujam, "Sequential estimation of optical properties of a two-layered epithelial tissue model from depth-resolved ultraviolet-visible diffuse reflectance spectra," Appl. Opt. **45**(19), 4776–4790 (2006).
7. R. Bays, G. Wagnières, D. Robert, D. Braichotte, J. F. Savary, P. Monnier, and H. van den Bergh, "Clinical determination of tissue optical properties by endoscopic spatially resolved reflectometry," Appl. Opt. **35**(10), 1756–1766 (1996).

#254728 Received 2 Dec 2015; revised 17 Jan 2016; accepted 18 Jan 2016; published 21 Jan 2016

8. R. M. Doornbos, R. Lang, M. C. Aalders, F. W. Cross, and H. J. Sterenborg, "The determination of in vivo human tissue optical properties and absolute chromophore concentrations using spatially resolved steady-state diffuse reflectance spectroscopy," Phys. Med. Biol. **44**(4), 967–981 (1999).
9. T. J. Farrell, M. S. Patterson, and B. Wilson, "A Diffusion Theory Model of Spatially Resolved, Steady-State Diffuse Reflectance for the Noninvasive Determination of Tissue Optical Properties Invivo," Med. Phys. **19**(4), 879–888 (1992).
10. M. Pilz, S. Honold, and A. Kienle, "Determination of the optical properties of turbid media by measurements of the spatially resolved reflectance considering the point-spread function of the camera system," J. Biomed. Opt. **13**(5), 054047 (2008).
11. Y. W. Chen and S. H. Tseng, "Efficient construction of robust artificial neural networks for accurate determination of superficial sample optical properties," Biomed. Opt. Express **6**(3), 747–760 (2015).
12. S. Coimbra, A. Santos-Silva, A. Figueiredo, H. Oliveira, and P. Rocha-Pereira, *Psoriasis: Epidemiology, Clinical and Histological Features, Triggering Factors, Assessment of Severity and Psychosocial Aspects* (INTECH Open Access Publisher, 2012).
13. S. R. Feldman and G. G. Krueger, "Psoriasis assessment tools in clinical trials," Ann. Rheum. Dis. **64**(Suppl 2), ii65–ii73 (2005).
14. S. A. Prahl, M. J. van Gemert, and A. J. Welch, "Determining the optical properties of turbid mediaby using the adding-doubling method," Appl. Opt. **32**(4), 559–568 (1993).
15. A. N. Bashkatov, E. A. Genina, V. I. Kochubey, and V. V. Tuchin, "Optical properties of human skin, subcutaneous and mucous tissues in the wavelength range from 400 to 2000 nm," J. Phys. D Appl. Phys. **38**(15), 2543–2555 (2005).
16. S. H. Tseng, C. K. Hsu, J. Yu-Yun Lee, S. Y. Tzeng, W. R. Chen, and Y. K. Liaw, "Noninvasive evaluation of collagen and hemoglobin contents and scattering property of in vivo keloid scars and normal skin using diffuse reflectance spectroscopy: pilot study," J. Biomed. Opt. **17**(7), 077005 (2012).
17. S. Jacques, "Melanosome absorption coefficient," (1998), *http://omlc.org/spectra/melanin/index.html*.
18. S. Prahl, "Hemoglobin absorption coefficient," (1999), *http://omlc.org/spectra/hemoglobin/summary.html*.
19. P. Taroni, A. Bassi, D. Comelli, A. Farina, R. Cubeddu, and A. Pifferi, "Diffuse optical spectroscopy of breast tissue extended to 1100 nm," J. Biomed. Opt. **14**(5), 054030 (2009).
20. S. H. Tseng, P. Bargo, A. Durkin, and N. Kollias, "Chromophore concentrations, absorption and scattering properties of human skin in-vivo," Opt. Express **17**(17), 14599–14617 (2009).
21. M. A. Lowes, A. M. Bowcock, and J. G. Krueger, "Pathogenesis and therapy of psoriasis," Nature **445**(7130), 866–873 (2007).
22. V. Koivukangas, M. Kallionen, J. Karvonen, H. Autio-Harmainen, J. Risteli, L. Risteli, and A. Oikarinen, "Increased collagen synthesis in psoriasis in vivo," Arch. Dermatol. Res. **287**(2), 171–175 (1995).
23. L. Panzella, K. Wakamatsu, G. Monfrecola, S. Ito, F. Ayala, and A. Napolitano, "Increased cysteinyldopa plasma levels hint to melanocyte as stress sensor in psoriasis," Exp. Dermatol. **20**(3), 288–290 (2011).
24. M. Leroy, T. Lefèvre, R. Pouliot, M. Auger, and G. Laroche, "Using infrared and Raman microspectroscopies to compare ex vivo involved psoriatic skin with normal human skin," J. Biomed. Opt. **20**(6), 067004 (2015).
25. C. Q. F. Wang, Y. T. Akalu, M. Suarez-Farinas, J. Gonzalez, H. Mitsui, M. A. Lowes, S. J. Orlow, P. Manga, and J. G. Krueger, "IL-17 and TNF Synergistically Modulate Cytokine Expression while Suppressing Melanogenesis: Potential Relevance to Psoriasis," J. Invest. Dermatol. **133**(12), 2741–2752 (2013).
26. I. Flisiak, P. Porebski, and B. Chodynicka, "Effect of psoriasis activity on metalloproteinase-1 and tissue inhibitor of metalloproteinase-1 in plasma and lesional scales," Acta Derm. Venereol. **86**(1), 17–21 (2006).
27. L. Z. Carrenho, C. G. Moreira, C. C. Vandresen, R. Gomes Junior, A. G. Gonçalves, S. M. Barreira, M. D. Noseda, M. E. Duarte, D. R. Ducatti, M. Dietrich, K. Paludo, D. A. Cabrini, and M. F. Otuki, "Investigation of anti-inflammatory and anti-proliferative activities promoted by photoactivated cationic porphyrin," Photodiagn. Photodyn. Ther. **12**(3), 444–458 (2015).

## 1. Introduction

Diffuse Reflectance Spectroscopy (DRS) is capable of recovering the chromophore concentrations, absorption and scattering properties of various tissues such as breast, skin, and brain [1–3]. The general configuration of a DRS system includes a light source, a photo-detector, and an optical fiber probe for light delivery. The DRS system setups employing continuous wave (CW) light as the light source are very common due to relative low cost and small footprint, and many groups have proposed the use of DRS systems equipping with a CW light source and a handheld optical fiber probe for diagnostic and/or monitoring purposes [1, 3–5]. By using wavelength constraints, assuming the scattering property of skin follows a power law decay with wavelength and skin absorption property contributed from hemoglobin and melanin, CW DRS systems with a single source to detector separation (SDS) has been demonstrated to be able to evaluate skin properties [4, 6]. On the other hand, to accurately retrieve skin absorption and reduced scattering coefficients without applying wavelength

#254728 Received 2 Dec 2015; revised 17 Jan 2016; accepted 18 Jan 2016; published 21 Jan 2016

constraints, spatially resolved CW DRS is usually required [3, 7–10]. The measured spatial variation of diffuse reflectance can be used to determine the absorption and reduced scattering coefficients of samples independently at each wavelength, and the spectral characteristics of the sample absorption can further be used to determine the concentrations of chromophores. The spatially resolved CW DRS method is especially favorable when the tissues under investigation do not follow scattering power law and/or the assumption of hemoglobin and melanin as main tissue chromophores does not hold. For example, in our previous study, we demonstrated an optimized spatially resolved CW DRS benchtop system for monitoring the variation of water, collagen, and hemoglobin of keloidal scars induced by treatments [3].

Although spatially resolved CW DRS can be more accurate in the sample optical properties quantification than other CW DRS setups, it requires a complex optical probe design and an optical switching mechanism for facilitating the collection of the diffuse reflectance at several SDSs; these requirements are attained with additional system cost and size which limit its wide application in the clinical setting. Based on the optimized DRS design we proposed earlier [11], we have developed a handheld, low-cost DRS system that can conveniently be used for the quantification of skin optical properties in the clinical setting. Compared to other spatially resolved CW DRS system, the major advantage of the proposed system is that the optical fiber probe, optical switch, and the light source are integrated into one component to greatly reduce the size and the cost of the system.

To understand the clinical applicability of our handheld DRS system, we carried out a pilot study to measure the skin properties of 11 patients with psoriasis using the handheld system. Psoriasis is characterized by hyperplasia of the epidermis, hyperkeratosis of the stratum corneum, dilated microvasculature in the upper dermis and infiltration of inflammatory cells in the epidermis and dermis. The diagnosis of psoriasis sometimes relies on skin biopsies for histopathological evaluation. There are several visual-assessment based approaches for measuring the severity of psoriasis, such as Psoriasis Area and Severity Index (PASI), National Psoriasis Foundation Psoriasis Score (NPF-PS), Physician's Global Assessment (PGA), Lattice System Physician's Global Assessment (LS-PGA) [12, 13]. Among them, the PASI scoring system is the most commonly used by dermatologists in Taiwan since it is the scoring system suggested by Taiwan National Health Insurance Administration. Thus, we employed PASI as the reference scoring system in this study. We will demonstrate in this study that perceptible changes, induced by hemoglobin, and non-perceptible changes, such as average scatterer size and collagen concentration, can both be quantified using our handheld DRS system. The measurement results were compared to the PASI scores rated by three clinicians to understand the potential of our handheld system in objective and quantitative psoriasis severity assessment.

## 2. Materials and methods

### *2.1 Handheld CW DRS system*

The setup of the handheld DRS system was derived from our benchtop DRS system reported previously which consisted of a broadband light source (HL2000, Ocean Optics, FL), an optical switch (1x6, Leoni, Germany), a spectrometer (QE65000, Ocean Optics, FL), and a custom optical fiber probe with optimized source-to-detector separations of 1 and 2 mm [11]. To reduce the system footprint and cost of the benchtop system, a handheld DRS system as shown in Fig. 1(a) was developed. It can be seen that a compact spectrometer (USB2000+ , Ocean Optics, FL) and several electronic parts are employed in the system. The complete layout of the system is depicted in Fig. 1(b). Notably in this system is a custom gadget that combined the functions of the light source, the optical switch, and the optical fiber probe of the benchtop DRS system, and its 3D model is shown in Fig. 1(c).

As illustrated in the Fig. 1(b), a miniature filament light bulb (blue colored device) purchased from a local electronic store was operated at 24V and 0.04A and was located close

#254728 Received 2 Dec 2015; revised 17 Jan 2016; accepted 18 Jan 2016; published 21 Jan 2016

to the distal end of the device. Two cylindrical channels (yellow channels shown in Fig. 1(c)) were opened on the gadget's aluminum case to deliver the light emitting from the light bulb to the sample-device contact interface. They had diameter and length of 500 μm and 3 mm, respectively, and had center to center separation of 1 mm (edge to edge separation of 0.5 mm). A slim metal sheet (green colored part in Fig. 1(c)) was placed between the two cylindrical channels and the light bulb. As depicted in the layout shown in Fig. 1(b), the metal sheet attached to a rod that was connected to a miniature solenoid valve controlled by a relay (LEG-3, Rayex, Taiwan), and the relay was connected to a microcontroller (Arduino UNO, Arduino, MA). The slim metal sheet in the system had two default positions and its position could be controlled by the microcontroller to selectively block the light output to either of the two cylindrical channels. A homemade step-up converter was employed to covert the 5V output of the Arduino board to 28V to drive the light bulb. A multimode fiber with 480-μm diameter and 0.22 numerical aperture was placed next to the light output channels to collect the diffuse reflectance and transmit it to a spectrometer (USB2000+ , Ocean Optics, FL) whose functional wavelength range was 400-1000 nm. The light collection fiber and the two source channels have separation of 1 and 2 mm, respectively. The spectrometer and the microcontroller board were connected to a laptop through two USB cables and controlled by a custom LabVIEW (National Instruments, TX) graphical user interface. This handheld DRS system weighted 790 grams, and had a length of 29 cm, a maximum width of 10 cm, and a height of 5 cm. The illustration of a medical professional using the handheld DRS system to examine the skin of a patient in the clinical setting is shown in Fig. 1(d).

#254728 Received 2 Dec 2015; revised 17 Jan 2016; accepted 18 Jan 2016; published 21 Jan 2016

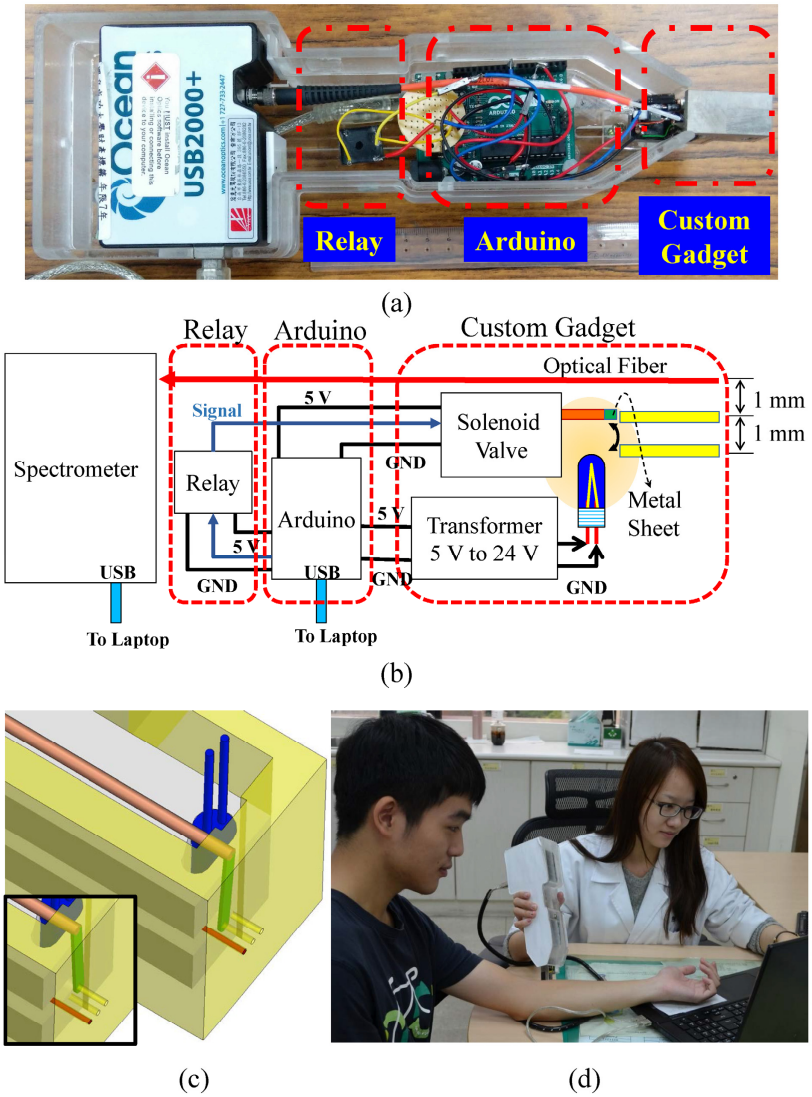


Fig. 1. (a) The handheld DRS system consists of spectrometer, a relay, a microcontroller board, and a custom gadget. (b) Schematics of the system configuration. A relay passes the Arduino control signal to the solenoid valve to change the position of a slim shield to switch light output. A step-up transformer converts the 5V supplied by the microcontroller board to 24V to drive the miniature filament bulb. An optical fiber directs the reflectance to a mini-spectrometer. The spectrometer and the Arduino board are connected to a laptop through USB cables. (c) A 3D model that illustrates the function of the slim metal sheet (green part) that attached to a metal rod. In one of its two default positions, the metal sheet prevents the light emitting from one of the two cylindrical channels. Inset shows the metal sheet in another default position. (d) Illustration of a medical professional using the handheld DRS system to examine the skin of a patient in the clinical setting.

### *2.2 Inverse model for optical properties recovery*

The inverse model for determining optical properties from the diffuse reflectance was an artificial neural network (ANN) trained by Monte Carlo simulation results. We have elaborated the key procedures for obtaining the ANN based inverse model and have validated the model thoroughly [11]. In brief, Monte Carlo simulations were carried out to calculate the

#254728 Received 2 Dec 2015; revised 17 Jan 2016; accepted 18 Jan 2016; published 21 Jan 2016

diffuse reflectance at 1 and 2 mm SDSs in the designed probing geometry. In the Monte Carlo model, the sample was assumed to be homogeneous and the sample optical properties were varied from 0.01 to 1.00 $mm^{-1}$ in a 0.01 $mm^{-1}$ step for $\mu_a$ and varied from 0.55 to 5.00 $mm^{-1}$ in a 0.05 $mm^{-1}$ step for $\mu_s'$. The sample refractive index of 1.43 and the Henyey-Greenstein phase function with anisotropy factor of 0.9 were used in the simulations. The simulation results were consolidated to form databases for the ANN training. Once the database was ready, we employed the MATLAB (Mathworks, MA) training function "*trainbr*" to construct the ANN inverse model.

### *2.3 Phantom study*

We fabricated two homogeneous silicone phantoms in which the Black India Ink and TiO2 powder were utilized as the absorbing and scattering agents, respectively. The benchmark optical properties of the two phantoms were determined by the inverse adding doubling method [14]. We employed one of the phantoms as the calibration phantom to determine the system response. Once the system response was obtained, we could determine the optical properties of the other phantom and evaluate the performance of the handheld DRS system.

### *2.4 In-vivo measurements on psoriatic skin*

Eleven subjects with active psoriasis were recruited in the National Cheng Kung University Hospital. The protocol was approved by the Institutional Review Board (No. ER-100-332) and the written informed consent was obtained from all subjects prior to the measurements. The photos of the measured lesion sites are illustrated in Fig. 2. The local severity of each psoriatic lesion was rated by three independent dermatologists using the PASI scoring system which includes the rating of erythema, thickness, scaling, and area. The erythema, thickness, and scaling scores were set in the range from 0 to 4 in which 0, 1, 2, 3, and 4 represented none, slight, moderate, severe, and very severe, respectively, and these scores of all subjects are listed in Table 1. The area of psoriatic lesions as the forth parameter of the PASI scoring system is not an apparent quantity related to DRS measurements and is not displayed here.

For each subject, measurements were taken at two sites including one site at the active psoriatic lesion (as indicated by arrows in Fig. 2) and one normal skin site which was several cm apart from the lesion. In this study, we chose psoriasis areas that were easily accessible with no hair, exfoliation, or wound. Each set of measurements was composed of 3 measuring repeats in which the probe was physically removed and gently replaced to the same point each time. Due to high noise level of the handheld system in the wavelength ranges from 400 to 500 nm and from 900 to 1000 nm, we only processed the data in the wavelength region from 500 to 900 nm. The derived reduced scattering spectra were fit to the scattering power law ($\mu_s' = a*\lambda^{-b}$) to smooth the curves and obtain the exponent "-b". The wavelength exponent "-b" characterizes the mean size of the tissue scatterers and larger "-b" values corresponds to larger scatterer diameters [15, 16].

The recovered absorption spectra were fit linearly to the known absorption spectra of oxygenated hemoglobin, deoxygenated hemoglobin, melanin, and collagen to extract the tissue chromophore concentrations [3, 17–19]. In the modeling of photon transport, it was assumed that the sample was homogeneous, and the recovered absorption coefficient had the unit of 1/mm. This means that the recovered absorption coefficient represented the average absorption of the probed region, and its unit suggests that the absorption coefficient derived was the total light absorption per mm. With known chromophore extinction coefficients translated in to proper units, we can use the Beer–Lambert law listed in the following form to estimate the chromophore concentrations of a sample:

$$\begin{aligned}\mu_{a(skin)}(\lambda) &= C_{HbO_2} \times \varepsilon_{HbO_2}(\lambda) + C_{Hb} \times \varepsilon_{Hb}(\lambda) \\ &+ C_{melanin} \times \varepsilon_{melanin}(\lambda) + C_{collagen} \times \varepsilon_{collagen}(\lambda),\end{aligned} \tag{1}$$

#254728 Received 2 Dec 2015; revised 17 Jan 2016; accepted 18 Jan 2016; published 21 Jan 2016

where C and ε represent the concentration and the extinction coefficient of chromophores, respectively. We did not include the absorption spectrum of water in Eq. (1) because there were no significant absorption features of water below 900 nm. The recovered hemoglobin concentrations were in micro Molar and the recovered concentrations of melanin and collagen were of arbitrary unit.

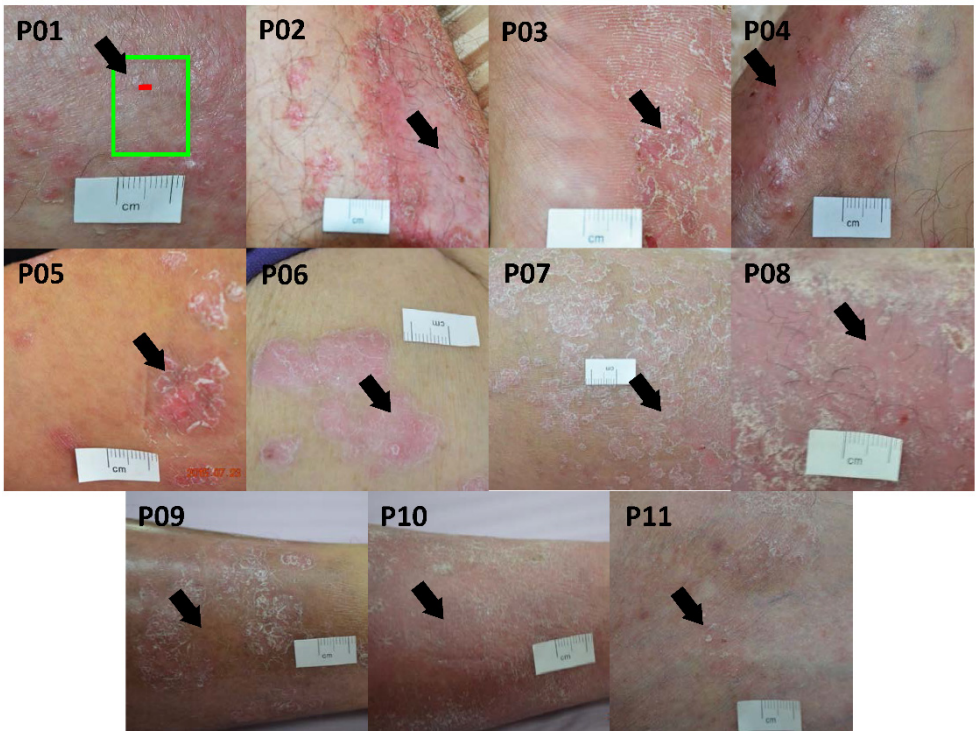


Fig. 2. Pictures of the psoriatic lesion of the 11 subjects recruited in this study. Arrows indicate the measurement sites. The green rectangle shows the probe contact area and the short red line represents the source-detector separation of 2mm.

**Table 1. The erythema, thickness, and scaling scores of the 11 subjects rated by 3 independent dermatologists.**

| Subject | Erythema score | | | Thickness score | | | Scaling score | | |
|---|---|---|---|---|---|---|---|---|---|
| | E_1 | E_2 | E_3 | T_1 | T_2 | T_3 | S_1 | S_2 | S_3 |
| P01 | 1 | 1 | 1 | 2 | 1 | 0 | 0 | 0 | 1 |
| P02 | 1 | 1 | 1 | 1 | 1 | 0 | 0 | 0 | 0 |
| P03 | 1 | 2 | 1 | 2 | 1 | 1 | 3 | 3 | 2 |
| P04 | 2 | 3 | 2 | 1 | 0 | 1 | 0 | 1 | 0 |
| P05 | 2 | 2 | 1 | 2 | 0 | 2 | 3 | 2 | 3 |
| P06 | 3 | 2 | 2 | 3 | 2 | 2 | 2 | 1 | 2 |
| P07 | 2 | 2 | 1 | 3 | 1 | 2 | 3 | 3 | 3 |
| P08 | 3 | 3 | 3 | 3 | 1 | 3 | 2 | 1 | 2 |
| P09 | 1 | 3 | 2 | 1 | 0 | 2 | 2 | 1 | 2 |
| P10 | 3 | 3 | 3 | 1 | 1 | 2 | 2 | 1 | 2 |
| P11 | 1 | 1 | 1 | 1 | 0 | 2 | 1 | 1 | 1 |

## 3. Results and discussion

### *3.1 Phantom validation results*

We designed a phantom study to evaluate the sample optical properties recovery accuracy of the handheld DRS system, and its performance was compared to that of the benchtop DRS system. The results are shown in Fig. 3. The benchmark optical properties of the silicone

#254728 Received 2 Dec 2015; revised 17 Jan 2016; accepted 18 Jan 2016; published 21 Jan 2016

phantom were determined from the inverse adding-doubling theory and are shown in black lines in Fig. 2. The optical properties recovered from the handheld and the benchtop DRS systems were illustrated in blue and red lines, respectively. Due to high noise level of the handheld system in the wavelength ranges from 400 to 500 nm and from 900 to 1000 nm, data in these wavelength ranges are not presented here. We found that in general the optical properties recovered from the two systems were very close. In the 600-900 nm region, the difference between the optical properties recovered from the two systems were less than 10%. However, in the 500-600 nm region, the benchtop system had less than 10% optical property recovery error, while the absorption coefficient recovery error of the handheld system could reach 20%. The inferior performance of the handheld system to that of the benchtop system in the 500-600 nm range was caused by the specification differences between the spectrometers and the light sources employed in the two systems. Overall, it can be seen in Fig. 3 that the handheld system delivers comparable results to those of the bench top system.

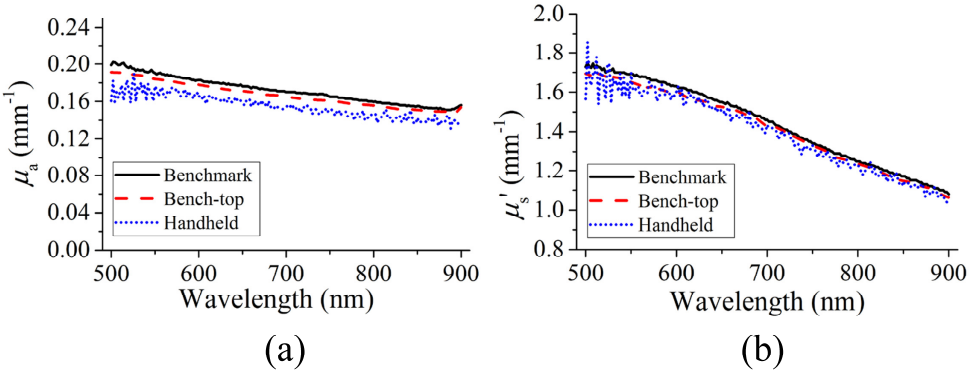


Fig. 3. (a) Absorption and (b) reduced scattering spectra of a silicone phantom. Black lines represent the benchmark values, and red dash and blue dot lines represent the values recovered from the benchtop and handheld systems, respectively.

### *3.2 Skin optical properties of psoriatic patients*

In the following subsections, the light absorption and scattering properties of psoriatic lesions versus normal appearing skin are presented. The correlation between these optical properties and the three parameters of PASI which reflect local severity of psoriasis, namely erythema, thickness and scaling, are also discussed.

#### 3.2.1 Absorption

The absorption spectra of the lesion (red dot lines) and normal (black lines) sites of two patients (P02 and P08) are displayed in Fig. 4. In Fig. 4(a) (subject P08), it can be seen that the absorption of lesion site is significantly higher than that of normal site in the wavelength range from 500 to 600 nm, while at wavelengths from 650 to 900 nm, the difference between the absorption of normal and psoriatic lesion is very little and almost not distinguishable. The marked elevation of the 500-600 nm absorption coefficients of the lesion site is majorly caused by the increase blood volume at the site as can be observed in the photograph of subject P08. On the other hand, the skin absorption spectra of subject P02 shown in Fig. 4(b) do not show significant differences ($p$ >0.05) between the lesion and normal sites in the 500-600 nm as well as 600-900 nm wavelength ranges; however, the average of absorption spectra of the lesion (0.342 mm$^{-1}$) is slightly higher than that of the normal skin (0.281 mm$^{-1}$) from 500 to 580 nm. It can be noticed from the results shown in Fig. 4 that the difference between the absorption of the lesion and normal sites could have divergent manifestation for different patients. In addition, we did not see the absorption and hemoglobin concentration of samples affected by the bulb's infrared spectrum or their increase during multiple measurements.

#254728 Received 2 Dec 2015; revised 17 Jan 2016; accepted 18 Jan 2016; published 21 Jan 2016

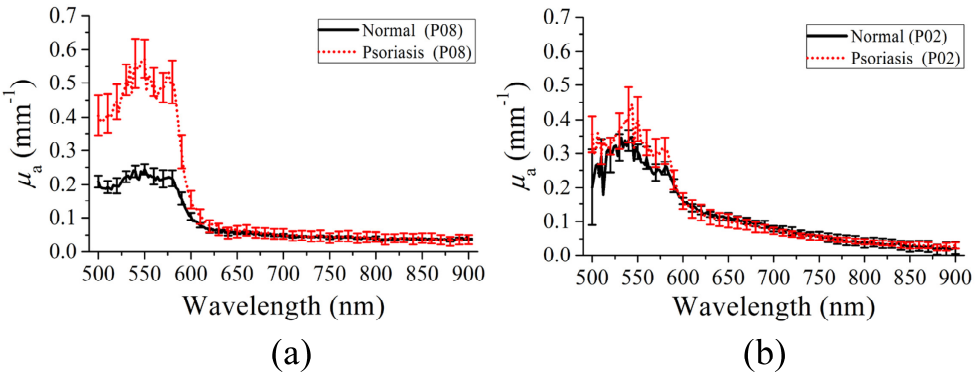


Fig. 4. Absorption spectra of (a) subject PS08 and (b) subject PS02. Black and red dot lines represent the absorption spectra recovered from normal and lesion sites, respectively. Error bars represent the standard deviation of the derived absorption spectra of a set of measurements.

The absorption coefficients of normal and lesion sites at 550 and 800 nm for all subjects are listed in Table 2. 550 nm is the medium wavelength that we chose for representing the high absorption wavelength region from 500 to 600 nm; on the other hand, 800 nm was chosen for representing the relative low absorption wavelength region from 700 to 900 nm. Besides, difference between the absorption coefficients of lesion and normal sites are also listed in the table. It can be observed in Table 2 that the absorption coefficients of lesion sites are in general higher than those of normal sites at 550 nm. Student's *t*-test was carried out for the 550 nm absorption coefficients of lesion and normal sites, and it was found that the two series were statistically distinguishable ($p$ = 0.0056). It has been reported that one of the prominent features of psoriatic lesion is the dilated microvasculature in the upper dermis; thus our results suggest that at 550 nm where hemoglobin exhibits strong absorption, our system could be sensitive to the altered upper dermis microvasculature of psoriasis. On the other hand, at 800 nm ($p$ = 0. 4253) the absorption differences between lesion and normal sites are not as significant as those at 550 nm ($p$ = 0.0056). As reported in our earlier study, the interrogation depth of a typical DRS system would be modulated by the wavelength region employed, and in the 500-900 nm region, the interrogation depth increases with the wavelength [20]; therefore, it can be inferred that the interrogation depth at 800 nm was deeper than that at 550 nm in this study. Thus, the probing volume at 800 nm could be too large in skin to effectively sensing the upper dermis microvasculature alteration of psoriasis.

**Table 2. Absorption coefficients of the lesion (P) and normal skin (N) at 550 and 800 nm of the 11 subjects. The absorption differences (Δ) between the lesion and normal skin are also listed.**

| Subject | $\mu_a$ (mm$^{-1}$) at 550 nm | | | $\mu_a$ (mm$^{-1}$) at 800 nm | | |
|---|---|---|---|---|---|---|
| | P | N | Δ | P | N | Δ |
| P01 | 0.168 | 0.144 | 0.025 | 0.027 | 0.014 | 0.014 |
| P02 | 0.401 | 0.305 | 0.096 | 0.041 | 0.038 | 0.003 |
| P03 | 0.237 | 0.181 | 0.056 | 0.031 | 0.025 | 0.006 |
| P04 | 0.309 | 0.250 | 0.059 | 0.058 | 0.046 | 0.013 |
| P05 | 0.359 | 0.315 | 0.044 | 0.027 | 0.034 | –0.007 |
| P06 | 0.354 | 0.244 | 0.110 | 0.017 | 0.030 | –0.014 |
| P07 | 0.361 | 0.369 | –0.009 | 0.046 | 0.076 | –0.030 |
| P08 | 0.573 | 0.244 | 0.328 | 0.044 | 0.043 | 0.001 |
| P09 | 0.599 | 0.188 | 0.411 | 0.041 | 0.027 | 0.014 |
| P10 | 0.335 | 0.146 | 0.189 | 0.033 | 0.018 | 0.015 |
| P11 | 0.376 | 0.319 | 0.057 | 0.018 | 0.020 | –0.002 |

To understand the relation between the measured absorption coefficients and the erythema scores, we calculated the correlation coefficients of erythema scores and the absorption

#254728 Received 2 Dec 2015; revised 17 Jan 2016; accepted 18 Jan 2016; published 21 Jan 2016

coefficient difference ($\Delta\mu_a$) between the lesion and normal sites at 550 and 800 nm as listed in Table 3. Interestingly, it can be noted that the erythema score series E_1 rated by one of the clinicians is not well correlated to the erythema score series E_2 and E_3 rated by the other two clinicians with correlation coefficients of around 0.5, while the erythema score series E_2 and E_3 have a relatively high correlation coefficient of 0.785. This suggests that there could be subjective factors in generating the erythema scores. Furthermore, we can find from Table 3 that the absorption coefficients difference between the lesion and normal sites at 550 nm has medium-high correlation coefficients to the erythema score series E_2 and E_3 but has a rather weak correlation coefficient to the score series E_1. On the other hand, the difference between the absorption coefficients at the lesion and normal sites at 800 nm is weakly correlated to all erythema score series. Since the dilated vasculature in the upper dermis at lesion sites produced increased absorption at 550 nm but not at 800 nm as discussed earlier, it is reasonable to see that the absorption differences at 800 nm are weakly correlated to the erythema scores.

**Table 3. Correlation coefficients of absorption differences at 550 and 800 nm and the erythema scores rated by 3 clinicians.**

| | $\Delta\mu_a$ (550 nm) | $\Delta\mu_a$ (800 nm) | E_1 | E_2 | E_3 |
|---|---|---|---|---|---|
| $\Delta\mu_a$ (550 nm) | | 0.41 | 0.20 | 0.62 | 0.69 |
| $\Delta\mu_a$ (800 nm) | 0.41 | | –0.25 | 0.23 | 0.33 |
| E_1 | 0.20 | –0.25 | | 0.50 | 0.55 |
| E_2 | 0.62 | 0.23 | 0.50 | | 0.79 |
| E_3 | 0.69 | 0.33 | 0.55 | 0.79 | |

### 3.2.2 Reduced scattering

The reduced scattering spectra of subjects P02 and P08 are illustrated in Fig. 5. It can be seen in Fig. 5 that for subject P08 the magnitude of reduced scattering of the normal site is significantly higher than that of the lesion site at all wavelengths, while the reduced scattering spectra of the lesion and normal sites of subject P02 are statistically indistinguishable ($p$ >0.05). From the two examples shown in Fig. 5, it seems that the relation between the scattering properties of psoriatic lesion and normal sites is not definite. The reduced scattering coefficients at the wavelengths of 550 and 800 nm as well as the wavelength exponent derived from the scattering power law fitting of all subjects are listed in Table 4.

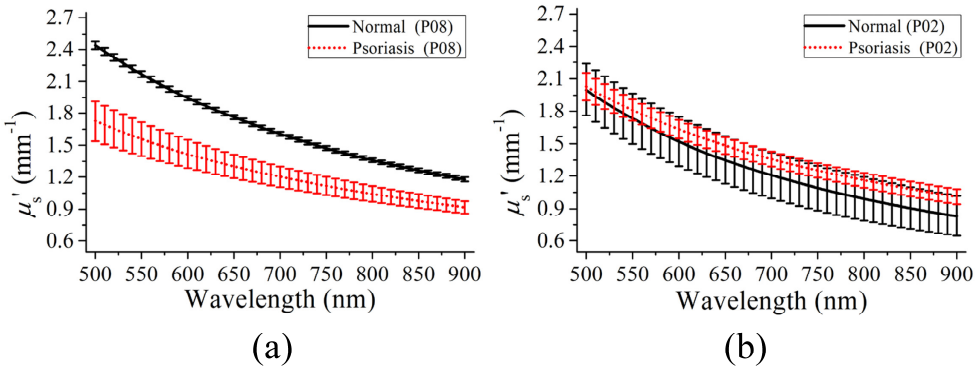


Fig. 5. Reduced scattering spectra of (a) subject P08 and (b) subject P02. Black and red dot lines represent the reduced scattering spectra recovered from normal and lesion sites, respectively. Error bars represent the standard deviation of the derived absorption spectra of a set of measurements.

#254728 Received 2 Dec 2015; revised 17 Jan 2016; accepted 18 Jan 2016; published 21 Jan 2016

**Table 4. Reduced scattering coefficients and the wavelength exponent "-b" of the lesion (P) and normal skin (N) of the 11 subjects. The scattering property differences (Δ) between the lesion and normal skin are also listed.**

| Subject | $\mu_s'$ (mm$^{-1}$) at 550 nm | | | $\mu_s'$ (mm$^{-1}$) at 800 nm | | | -b | | |
|---|---|---|---|---|---|---|---|---|---|
| | P | N | Δ | P | N | Δ | P | N | Δ |
| P01 | 3.267 | 3.912 | –0.645 | 2.301 | 2.557 | –0.256 | –1.00 | –1.10 | 0.10 |
| P02 | 1.811 | 1.732 | 0.079 | 1.160 | 0.990 | 0.170 | –1.14 | –1.67 | 0.53 |
| P03 | 2.280 | 1.700 | 0.581 | 1.505 | 0.974 | 0.531 | –1.12 | –1.49 | 0.37 |
| P04 | 2.027 | 2.242 | –0.215 | 1.498 | 1.573 | –0.076 | –0.77 | –0.95 | 0.18 |
| P05 | 2.003 | 2.349 | –0.346 | 1.267 | 1.512 | –0.244 | –1.22 | –1.15 | –0.07 |
| P06 | 1.978 | 2.361 | –0.384 | 1.171 | 1.469 | –0.298 | –1.40 | –1.27 | –0.13 |
| P07 | 1.847 | 2.294 | –0.447 | 1.167 | 1.526 | –0.358 | –1.16 | –1.09 | –0.07 |
| P08 | 1.488 | 2.168 | –0.680 | 1.010 | 1.361 | –0.352 | –1.03 | –1.23 | 0.20 |
| P09 | 1.614 | 1.822 | –0.208 | 1.147 | 1.197 | –0.050 | –0.92 | –1.13 | 0.21 |
| P10 | 1.979 | 2.427 | –0.448 | 1.354 | 1.437 | –0.083 | –1.01 | –1.40 | 0.39 |
| P11 | 2.215 | 2.112 | 0.102 | 1.403 | 1.375 | 0.028 | –1.26 | –1.14 | –0.12 |

It can be seen in Table 4 that the lesion site has lower reduced scattering than does the normal site for most subjects recruited at 550 and 800 nm. On the other hand, higher wavelength exponent "-b" at the lesion site than at the normal site for most subjects can be observed. We ran Student's *t*-test and found that among all scattering properties recovered only the "-b" parameters of lesion and normal sites had significant difference ($p$ <0.05). Our finding suggests that tissue structure and/or content of psoriatic lesions would be different from those of normal skin. It has been reported in the literature that the psoriatic skin has expanded vessel size and elevated number of aggregates of leukocytes in the dermis [21], and these alterations in the tissue could increase the average scatterer size which would in turn raise the value of wavelength exponent.

Further, to understand correlation between the scattering properties and the appearance scores rated by dermatologists, the correlation coefficients of three clinical scores and the scattering property difference ($\Delta\mu_s'$) between the lesion and normal sites were calculated and are listed in Table 5. However, good and consistent correlation between any of the scattering properties and any clinical score series rated by the clinicians cannot be observed as shown in the table. This suggests that the scattering property could be useful for detecting the microscopic structural or spatial changes in psoriasis, but could not reflect the clinical severity as inspected visually by clinicians.

**Table 5. Correlation coefficients of scattering property differences and the appearance scores rated by 3 clinicians.**

| | E_1 | E_2 | E_3 | T_1 | T_2 | T_3 | S_1 | S_2 | S_3 |
|---|---|---|---|---|---|---|---|---|---|
| $\Delta\mu_s'$ (550 nm) | –0.59 | –0.28 | –0.47 | –0.40 | –0.18 | –0.32 | 0.07 | 0.32 | –0.24 |
| $\Delta\mu_s'$ (800 nm) | –0.58 | –0.19 | –0.31 | –0.51 | –0.13 | –0.44 | –0.04 | 0.17 | –0.34 |
| -b | –0.17 | 0.17 | 0.23 | –0.46 | 0.07 | –0.42 | –0.25 | –0.23 | –0.42 |

### *3.3 Skin chromophore concentrations*

Chromophore concentrations of skin including oxy-hemoglobin, deoxy-hemoglobin, melanin, and collagen were determined from the absorption spectra of all subjects, and the values are listed in Table 6. The differences between the chromophore concentrations of lesion and normal sites are also displayed in the table. It was found that oxy-hemoglobin, deoxy-hemoglobin, and total hemoglobin (not listed in Table 6) concentrations of the lesion sites of all subjects had statistically difference ($p$<0.05, Student's pair *t*-test) from those of normal skin of all subjects. Since psoriasis typically has enlarged vessels in the upper dermis, it is natural to find hemoglobin concentrations are significantly different between psoriasis and normal skin. In contrast, local tissue oxygen saturation (not listed in Table 6) and melanin and collagen concentrations of the lesion and normal sites of the 11 subjects were not statistically

#254728 Received 2 Dec 2015; revised 17 Jan 2016; accepted 18 Jan 2016; published 21 Jan 2016

different ($p$ = 0.06 for oxygen saturation, $p$ = 0.16 for melanin, and $p$ = 0.50 for collagen). We have found unreconciled conclusions from literatures regarding the difference in melanin and collagen content between psoriasis and unaffected skin. While some of the literatures have pointed out that skin melanocyte activity and collagen synthesis might be positively correlated to the severity of psoriasis [22, 23], others reported inhibited melanin production or unchanged collagen distribution of psoriatic lesions [24, 25]. Our results shown here suggest that these two chromophore concentrations derived from optical measurements might not be effective factors for the diagnosis of psoriasis.

**Table 6. Chromophore concentrations including oxy-hemoglobin, deoxy-hemoglobin, melanin, and collagen, of the lesion (P) and normal skin (N) of the 11 subjects. The chromophore concentration differences (Δ) between the lesion and normal skin are also listed.**

| Subject | $HbO_2$ | | | Hb | | | Melanin | | | Collagen | | |
|---|---|---|---|---|---|---|---|---|---|---|---|---|
| | P | N | Δ | P | N | Δ | P | N | Δ | P | N | Δ |
| P01 | 4.20 | 3.51 | 0.69 | 9.65 | 7.83 | 1.82 | 0.07 | 0.06 | 0.01 | 3.77 | 0.82 | 2.95 |
| P02 | 12.26 | 9.19 | 3.07 | 14.36 | 13.56 | 0.81 | 0.27 | 0.19 | 0.07 | 4.86 | 4.32 | 0.53 |
| P03 | 12.19 | 9.35 | 2.84 | 8.12 | 5.80 | 2.32 | 0.06 | 0.07 | –0.01 | 3.55 | 2.79 | 0.76 |
| P04 | 5.68 | 6.99 | –1.30 | 13.62 | 10.99 | 2.63 | 0.34 | 0.22 | 0.12 | 8.66 | 6.80 | 1.86 |
| P05 | 20.51 | 11.37 | 9.13 | 11.15 | 12.89 | –1.75 | 0.10 | 0.19 | –0.09 | 3.94 | 4.93 | –0.99 |
| P06 | 13.10 | 4.10 | 9.00 | 13.48 | 12.09 | 1.39 | 0.23 | 0.25 | –0.02 | 1.34 | 4.05 | –2.71 |
| P07 | 11.81 | 7.04 | 4.76 | 14.97 | 19.92 | –4.95 | 0.35 | 0.33 | 0.02 | 6.40 | 10.96 | –4.56 |
| P08 | 18.68 | 6.48 | 12.20 | 23.79 | 11.43 | 12.36 | 0.25 | 0.13 | 0.11 | 5.38 | 5.25 | 0.13 |
| P09 | 11.98 | 3.55 | 8.43 | 27.45 | 6.58 | 20.87 | 0.57 | 0.28 | 0.29 | 3.51 | 3.76 | –0.25 |
| P10 | 16.73 | 3.95 | 12.78 | 15.67 | 6.46 | 9.20 | 0.19 | 0.12 | 0.07 | 4.55 | 1.67 | 2.89 |
| P11 | 14.84 | 8.72 | 6.11 | 14.75 | 14.68 | 0.07 | 0.18 | 0.19 | –0.01 | 1.37 | 2.06 | –0.70 |

The correlation coefficients of lesion erythema scores and the differences between the hemoglobin parameters of the lesion and normal sites were calculated, and the values are presented in Table 7. Interestingly, it can be seen that the total hemoglobin and deoxygenated hemoglobin concentration differences (Δ(THb), Δ(Hb)) have low correlation to one of the erythema score series (E_1) but has medium to medium-high correlation to the rest two score series (E_2 and E_3). This suggests that hemoglobin related property differences could be used as the objective markers to evaluate erythema of psoriasis.

**Table 7. Correlation coefficients of hemoglobin related property differences between the lesion and normal sites and the erythema scores rated by 3 clinicians.**

| | E_1 | E_2 | E_3 |
|---|---|---|---|
| $\Delta(HbO_2)$ | 0.63 | 0.42 | 0.62 |
| Δ(Hb) | 0.08 | 0.63 | 0.67 |
| Δ(THb) | 0.34 | 0.64 | 0.76 |
| $\Delta(SaO_2)$ | 0.53 | –0.20 | 0.00 |

In addition, the correlation coefficients of concentration difference in melanin and collagen between lesion and normal sites and the appearance scores were determined and listed in Table 8. In Table 8, it can be observed that the melanin concentration difference has medium correlation to the erythema score series rated by two of the clinicians, and it has low correlation to the thickness and scaling scores. This suggests that the melanin concentration of skin might bias the rating of the erythema scores but not the other two appearance scores.

Moreover, it was found that the collagen concentration difference had very low correlation to the erythema scores. Interestingly, we observed that the collagen concentration difference had negative medium correlation to all of the scaling score series. Our results

#254728 Received 2 Dec 2015; revised 17 Jan 2016; accepted 18 Jan 2016; published 21 Jan 2016

suggests that the collagen concentration decreased as the lesion site got higher scaling scores. It has been shown that the collagen metalloproteinase would be higher for patients with higher PASI scores [26], and this implies that the collagen content would decrease as the PASI score increases. Our results seem to be in line with those reported in the literature. Further investigation will be carried out to find out the correlation between the skin collagen content and the presentation of skin thickness and scaling at the lesion site which are linked to the inflammatory and proliferative activities of psoriasis [27].

**Table 8. Correlation coefficients of melanin and collagen concentration differences between the lesion and normal sites and the appearance scores rated by 3 clinicians.**

| | E_1 | E_2 | E_3 | T_1 | T_2 | T_3 | S_1 | S_2 | S_3 |
|---|---|---|---|---|---|---|---|---|---|
| Δ(Melanin) | –0.09 | 0.56 | 0.50 | –0.37 | –0.27 | 0.11 | –0.22 | –0.31 | –0.24 |
| Δ(Collagen) | –0.15 | 0.10 | 0.27 | –0.58 | –0.18 | –0.45 | –0.54 | –0.53 | –0.54 |

## 4. Conclusion

In this study, we demonstrated a handheld DRS system whose footprint and total cost were much less than a typical benchtop DRS system. The merits of the handheld system were achieved through a custom designed gadget that integrated the function of a light source, an optical switch, and an optical fiber probe. The accuracy in sample optical property recovery of the handheld system was carefully validated through a phantom study, and it was found that the performance of the system was similar to a benchtop system.

The small footprint and ease of use of the handheld DRS system would facilitate its application in clinical studies. We employed the handheld system to study the optical properties of psoriatic skin of 11 patients. The absorption, reduced scattering, and chromophore concentrations were calculated for the normal and lesion sites. The derived property differences between the normal and lesion sites were compared to the lesion appearance scores rated by three dermatologists. It was found that in general the absorption coefficient at 550 nm and the total hemoglobin concentration were well correlated to the erythema scores. The melanin concentration difference had low correlation to the thickness and scaling scores, and had medium correlation to the erythema score series rated by two of the clinicians. The collagen concentration difference had negative medium correlation to all of the scaling and thickness score series rated by two of the clinicians. Consistent correlation between the scattering properties and any of the clinical score series could not be observed. In addition, although the wavelength exponents, derived from the scattering power law fitting to the reduced scattering spectra, for the normal and lesion sites were statistically distinct, indicating the significant scatterers size difference between the two sites, they were not well correlated to any of the clinical scores. We also noted that the optical measurement results had poor correlation to the mean appearance scores of all three dermatologists. Overall, our finding suggested that the optical measurement results containing both visually perceptible and imperceptible information could assist the clinical diagnosis or evaluation of psoriasis without performing invasive histopathology examination. Our preliminary results indicate that the handheld system has the potential of being widely used in the clinical setting as a convenient tool for objective evaluation of psoriasis. Future studies to include a larger number of subjects would be necessary to verify our present findings.

## Acknowledgment

This research was supported by the Ministry of Science and Technology of Taiwan under Grant No. 104-2221-E-006-179-MY3. We thank Drs. Cheng-Han Liu, Chaw-Ning Lee and Fu-Nien Hsieh from the Department of Dermatology, National Cheng Kung University Hospital for rating PASI scores.

#254728 Received 2 Dec 2015; revised 17 Jan 2016; accepted 18 Jan 2016; published 21 Jan 2016